A&A 573, A114 (2015)
DOI: 10.1051/0004-6361/201424654

Astronomy & Astrophysics

Mapping possible non-Gaussianity in the *Planck* maps

A. Bernui[1] and M. J. Rebouças[2]

[1] Observatório Nacional, Rua General José Cristino 77, 20921-400 Rio de Janeiro – RJ, Brazil
e-mail: bernui@on.br
[2] Centro Brasileiro de Pesquisas Físicas, Rua Dr. Xavier Sigaud 150, 22290-180 Rio de Janeiro – RJ, Brazil
e-mail: reboucas@cbpf.br

Received 22 July 2014 / Accepted 6 October 2014

ABSTRACT

Context. The study of the non-Gaussianity of the temperature fluctuations of cosmic background radiation (CMB) can be used to break the degeneracy between the inflationary models and to test alternative scenarios of the early universe. However, there are several sources of non-Gaussian contaminants in the CMB data, which make a convincing extraction of primordial non-Gaussianity into an ambitious observational and statistical enterprise. It is conceivable that no single statistical estimator can be sensitive to all forms and levels of non-Gaussianity that may be present in observed CMB data. In recent works a statistical procedure based upon the calculation of the skewness and kurtosis of the patches of CMB sky sphere has been proposed and used to find out significant large-angle deviation from Gaussianity in the foreground-reduced WMAP maps.
Aims. Here we address the question of how previous recent analyses of Gaussianity of WMAP maps are modified if the nearly full-sky foreground-cleaned *Planck* maps are used, therefore extending and complementing such an examination in several regards.
Methods. Once the foregrounds are cleaned through different component separation procedures, each of the resulting *Planck* maps is then tested for Gaussianity. We determine quantitatively the effects for Gaussianity when masking the foreground-cleaned *Planck* maps with the INPMASK, VALMASK, and U73 *Planck* masks.
Results. We show that although the foreground-cleaned *Planck* maps present significant deviation from Gaussianity of different degrees when the less severe INPMASK and VALMASK are used, they become consistent with Gaussianity as detected by our indicator S when masked with the union U73 mask. A slightly smaller consistency with Gaussianity is found when the K indicator is employed, which seems to be associated with the large-angle anomalies reported by the *Planck* team. Finally, we examine the robustness of the Gaussianity analyses with respect to the real pixel's noise as given by the *Planck* team, and show that no appreciable changes arise when it is incorporated into the maps. The results of our analyses provide important information concerning Gaussianity of the foreground-cleaned *Planck* maps when diverse cut-sky masks are used.

Key words. cosmic background radiation – cosmology: observations

1. Introduction

The most general spacetime geometry consistent with the principle of spatial homogeneity and isotropy and the existence of a cosmic time is the Friedmann-Lemaître-Robertson-Walker (FLRW) metric. Within the FLRW approach to cosmological modeling in the framework of general relativity, the additional suggestion that the Universe underwent a period of rapid accelerating expansion (Starobinsky 1979a,b, 1982; Kasanas 1980; Sato 1981; Guth 1981; Linde 1982; Albrecht & Steinhardt 1982) has become an essential building block of the standard cosmological model. Besides solving the so-called horizon and flatness problems that come out in the FLRW model, the cosmological inflation provides a mechanism for the production of the primordial density fluctuations, which seeded the observed cosmic microwave background (CMB) anisotropies and the formation of large structures we observe in the Universe.

However, there are a great number of inflationary models, among which the simplest ones are based on a slowly-rolling single scalar field (see, for example, Bassett et al. 2006; Linde 2008). An important prediction of these simple models is that, regardless of the form of the kinetic term, the potential, or the initial vacuum state, they can generate only tiny primordial non-Gaussianity (Creminelli & Zaldarriaga 2004; Komatsu 2010). Thus, although convincing detection of a fairly large primordial non-Gaussianity would not exclude all inflationary models, it would rule out the entire class of simple models (see, e.g., Bartolo et al. 2004; Komatsu et al. 2009; Bassett et al. 2006). Moreover, robust stringent constraints on primordial non-Gaussianity would rule out alternative models of the early universe (see, for example, Koyama et al. 2007; Buchbinder et al. 2008; Lehners & Steinhardt 2008; Cai et al. 2009a,b). In this way, the study of primordial non-Gaussianity offers an important window into the physics of the early universe.

Gravitational waves generated by inflation provide another crucial window since they induce local quadrupole anisotropies in the radiation bombarding free electrons within last-scattering surface, inducing polarization in the scattered CMB photons. This polarized radiation includes the B-mode component that cannot be generated by density perturbations. Thus, detection of primordial B-mode polarization of CMB provides a unique confirmation of a crucial prediction of the simple inflationary models. Report of the detection of this B-mode polarization in the CMB has recently been made by BICEP Collaboration (Ade et al. 2014). But since the BICEP2's announcement, concerns about the impact of our Galaxy's dust contribution to the BICEP2 results have been raised (see, for example, Flauger et al. 2014 and Planck Collaboration XXX 2015).

In the study of deviation from Gaussianity of the CMB temperature fluctuations data, one is particularly interested in the

primordial component. However, there are several sources of non-Gaussianity in the observed CMB data that do not have a primordial origin, including contributions from residual diffuse foreground emissions (Bennett et al. 2003; Leach et al. 2008; Rassat et al. 2014), unresolved point sources (Komatsu et al. 2003), and systematic instrumental effects (Donzelli et al. 2009; Su et al. 2011), secondary CMB anisotropies, such as the Sunyaev-Zel'dovich effect (Zel'dovich & Sunyaev 1969; Novaes & Wuensche 2012), gravitational lensing (see Lewis & Challinor 2006 for a review), and the integrated Sachs-Wolfe effect (Rees & Sciama 1968)[1]. These contaminant non-Gaussian sources make a reliable extraction of primordial non-Gaussianity into a challenging observational and statistical enterprise.

Since there is no unique signature of non-Gaussianity, it is conceivable that no single statistical estimator can be sensitive to all sources of non-Gaussianity that may be present in observed CMB data. Furthermore, different statistical tools can provide valuable complementary information about different features of non-Gaussianity. Thus, is it important to test CMB data for deviations from Gaussianity by employing different statistical estimators to examine the non-Gaussian signals in the *Planck* CMB data and, possibly, to shed light on their source. The Planck collaboration has analyzed non-Gaussianity by using two classes of statistical tools (Planck Collaboration I, XXIII, XXIV 2014). In the first, the parametric optimal analyses were carried out to constrain the model-dependent amplitude parameter $f_{\rm NL}$ for the local, equilateral, and orthogonal bispectrum types. An important consistency with Gaussianity, at 1σ confidence level, has been found by narrowing considerably the *Wilkinson* Microwave Anisotropy Probe (WMAP) interval of $f_{\rm NL}$ for the three types (shapes) of non-Gaussianity (Planck Collaboration XXIV 2014). The second class contains a number of model-independent tools, including the spherical Mexican-hat wavelet (Martínez-González 2002), Minkowski functionals (Minkowski 1903; Gott et al. 1990; Komatsu et al. 2003, 2009; Eriksen et al. 2004; De Troia et al. 2007; Curto et al. 2008; Novaes et al. 2014), and the surrogate statistical technique (Räth et al. 2009, 2011; Modest et al. 2013). Little evidence of non-Gaussianity was obtained through most of these former indicators, but there are non-Gaussianity tools, such as the surrogate map technique, which suggests significant deviation from Gaussianity in CMB *Planck* data (Planck Collaboration XXIII 2014).

One of the simplest Gaussianity tests of a CMB map can be made by computing the skewness and kurtosis from the whole set of accurate temperature fluctuations values. This procedure would furnish two dimensionless overall numbers for describing Gaussianity, which could be compared, e.g., with the values of the statistical moments calculated from Gaussian simulated maps. The Planck collaboration has employed this procedure by calculating a sample of values of the skewness and kurtosis from the four foreground-cleaned U73-masked *Planck* maps, and made a comparison with the averaged values for the statistical moments obtained from simulated maps (Planck collaboration XXIII 2014)[2].

However, one can go a step further and obtain a large number of values of the skewness and kurtosis along with directional and angular-scale information about large-angle non-Gaussianity if one divides the CMB sphere $\mathbb{S}^2$ into a number j (say) of uniformly distributed spherical patches of equal area that cover $\mathbb{S}^2$. We then calculate the skewness, S_j, and the kurtosis, K_j, for each patch $j = 1, \ldots, n$. The union of values S_j and K_j can thus be used to define two discrete functions $S(\theta, \phi)$ and $K(\theta, \phi)$ in such way that $S(\theta_j, \phi_j) = S_j$ and $K(\theta_j, \phi_j) = K_j$ for every $j = 1, \ldots, n$. This is a constructive way of defining two discrete functions from any given CMB maps, which provide local measurements of the non-Gaussianity as a function of angular coordinates (θ, ϕ). The Mollweide projections of $S(\theta_j, \phi_j)$ and $K(\theta_j, \phi_j)$ are skewness and kurtosis maps, whose power spectra can be used to study two large-angle deviation from Gaussianity.

This statistical procedure based upon calculating the skewness and kurtosis of the patches of CMB sky sphere has recently been proposed in Bernui & Rebouças (2009) and used to examine deviation from Gaussianity in simulated maps (Bernui & Rebouças 2012), as well as in the foreground-reduced WMAP maps (Bernui & Rebouças 2010; see also Zhao 2013; Bernui et al. 2007). We note that these estimators capture directional information of non-Gaussianity and are useful in the presence of anisotropic signals, as foregrounds, for example. A pertinent question that arises here is how the analysis of Gaussianity made with WMAP maps is modified if the foreground-cleaned maps recently released by Planck collaboration are used. Our primary objective in this paper is to address this question by extending and complementing the analyses of Bernui & Rebouças (2010) in four different ways. First, we use the same statistical indicators to carry out a new analysis of Gaussianity of the available nearly full-sky foreground-cleaned *Planck* maps, which have been produced from CMB *Planck* observations in the nine frequency bands between 30 GHz and 875 GHz through different component separation techniques. Second, since the foregrounds are cleaned through different component separation procedures, each of the resulting foreground-cleaned *Planck* maps is thus tested for Gaussianity. Then, we make a quantitative analysis of the effects of different component separation cleaning methods in the Gaussianity and quantify the level of non-Gaussianity for each foreground-cleaned *Planck* map. Third, we quantitatively study the effects for the analyses of Gaussianity of masking the foreground-cleaned *Planck* maps with their INPMASK, VALMASK, and U73 masks. Fourth, we use *Planck* pixel's noise maps to examine the robustness of the Gaussianity analyses with respect to the pixel's noise as given by *Planck* team. These analyses of deviation from Gaussianity in the *Planck* maps provide important information about the suitability of the *Planck* maps as Gaussian reconstructions of the CMB sky, when diverse cut-sky masks are used.

The structure of the paper is as follows. In Sect. 2 we briefly present the *Planck* foreground-cleaned maps and the masks we use in this paper. In Sect. 3 we present our non-Gausssianity statistical indicators and the associated skewness and kurtosis maps. Section 4 contains the results of our analyses with-the foreground-cleaned *Planck* maps, and finally in Sect. 5 we present the summary of our main results and conclusions.

2. Foreground-cleaned maps and masks

Planck satellite has scanned the entire sky in nine frequency bands centered at 30, 44, 70, 100, 143, 217, 353, 545, and 857 GHz with angular resolution varying from ∼30 to ∼5 arcmin. These observations have allowed Planck collaboration to reconstruct the CMB temperature fluctuations over nearly the full sky. To this end, they used four different component

[1] The combination of the ISW and gravitational lensing produces the dominant contamination to the non-Gaussianity of local type (Goldberg & Spergel 1999).

[2] Different values for $N_{\rm side}$ were used by *Planck* team to show the robustness of their results with respect to the angular resolution of CMB maps.

Table 1. Sky fraction $f_{\rm sky}$.

Planck mask	$f_{\rm sky}$
SMICA – INPMASK	0.97
SMICA – VALMASK	0.89
NILC – INPMASK	0.97
NILC – VALMASK	0.93
SEVEM – VALMASK	0.76
U73 – UNION-MASK	0.73

separation techniques, aimed at removing the contaminants, including emissions from the Galaxy, which are present on large angular scales, and extragalactic foregrounds (and compact sources), which are dominant on small scales. These techniques are based on two different methodological approaches. In the first, only minimal assumptions about the foregrounds are made, and it is sought to minimize the variance of CMB temperature fluctuations for a determined blackbody spectrum, while the second essentially relies on parametric modeling of the foreground. By using the component separation techniques Planck collaboration produced four and released three nearly full-sky foreground-cleaned CMB maps (Planck Collaboration XII 2014), which are called SMICA (spectral matching independent component analysis, Cardoso et al. 2008), NILC (needlet internal linear combination, Delabrouille et al. 2009), SEVEM (spectral estimation via expectation maximization, Fernández-Cobos et al. 2012).

Each CMB *Planck* map is accompanied by its own confidence mask or validation mask (VALMASK, for short), outside which one has the pixels whose values of the temperature fluctuations are expected to be statistically robust and to have a negligible level of foreground contamination. Since the component separation techniques handle the data differently, the corresponding VALMASKs are different for each foreground-cleaning map-making procedure. Besides the VALMASKs, the SMICA and NILC maps were released with their corresponding minimal masks, called INPMASKs.

The allowed sky fraction for a given mask, i.e. the fraction of unmasked data pixels, is denoted by $f_{\rm sky}$. In Table 1 we collect the $f_{\rm sky}$ values, which give the fraction of unmasked pixels for the three foreground-cleaned *Planck* maps that we used in the statistical analyses of this article. Thus, for example, for the mask called U73, which is the union of the confidence masks, one has $f_{\rm sky} = 0.73$, since it allows only 73% of the CMB sky.

In addition to the above-mentioned foreground-cleaned maps and associated masks,the *Planck* team has produced and released noise maps that contain an estimate of the pixel's noise, particularly from the non-uniform strategy for scanning the CMB sky and noise of instrumental nature.

3. Non-Gaussianity statistical procedures and indicators

In this section we describe two non-Gaussian statistical indicators and the procedure for calculating their associated maps from CMB temperature fluctuations maps. The procedure described here is used in the following sections to investigate large-angle deviation from Gaussianity in the foreground-cleaned *Planck* maps.

Our primary purpose is to give a procedure for defining, from a given CMB map, two discrete functions, $S(\theta_j, \phi_j)$ and $K(\theta_j, \phi_j)$, on the two-sphere $\mathbb{S}^2$ that measure deviation from Gaussianity in the directions given by (θ_j, ϕ_j), where (θ, ϕ) are spherical coordinates and $j = 1, \ldots, n$ for a chosen integer n. The Mollweide projections of these two functions give what we call S and K maps, whose large scale features are employed to investigate large-angle deviation from Gaussianity.

To construct such functions, a first important ingredient is that deviation from Gaussianity of the CMB temperature fluctuations data can be measured by calculating the skewness S and the kurtosis K from temperature fluctuations data in patches, which are subsets of the CMB sky-sphere containing a number of pixels with their corresponding data values.

The second essential ingredient in the practical construction of $S(\theta_j, \phi_j)$ and $K(\theta_j, \phi_j)$ is the choice of these patches, to calculate S and K from the data therein. Here we chose these patches to be spherical caps (calottes) of aperture γ, centered on homogeneously distributed points on the CMB two-sphere $\mathbb{S}^2$. This choice was made in Bernui & Rebouças (2009, 2010, and 2012).

The above-outlined points of the procedure to define the discrete functions $S(\theta_j, \phi_j)$ and $K(\theta_j, \phi_j)$ from a given CMB map can be formalized through the following steps:

i. Take on the CMB two-sphere $\mathbb{S}^2$ a discrete set of n points homogeneously distributed as the centers of spherical caps of a given aperture γ (say);

ii. Using the values of the temperature fluctuations of a given CMB map, calculate, for each cap of the above item i, the skewness and kurtosis given, respectively, by

$$S_j = \frac{1}{N_{\rm p}\,\sigma_j^3} \sum_{i=1}^{N_{\rm p}} \left(T_i - \overline{T}_j \right)^3 , \tag{1}$$

$$K_j = \frac{1}{N_{\rm p}\,\sigma_j^4} \sum_{i=1}^{N_{\rm p}} \left(T_i - \overline{T}_j \right)^4 - 3, \tag{2}$$

for $j = 1, 2, \ldots, n$, and where $N_{\rm p}$ is the number of pixels in the jth cap; T_i is the temperature at the ith pixel in the jth cap; $\overline{T}_i$ the CMB mean temperature in the jth cap; and σ_j the standard deviation for the temperature fluctuations data of the jth cap.
Clearly, the values S_j and K_j obtained in this way for each cap give a measure of non-Gaussianity in the direction (θ_j, ϕ_j) of the center of each jth cap.

iii. Finally, use the union of all calculated values S_j to define a discrete function $S(\theta, \phi)$ on the two-sphere such that $S(\theta_j, \phi_j) = S_j$ for $j = 1, \ldots, n$. Similarly use the values K_j to define another discrete function $K(\theta, \phi)$ on $\mathbb{S}^2$ through the equation $K(\theta_j, \phi_j) = K_j$ for $j = 1, \ldots, n$. The Mollweide projection of these functions constitutes skewness and kurtosis maps, hereafter denoted as S-maps and K-maps, respectively, which we use to investigate the deviation from Gaussianity as a function of the angular coordinates (θ, ϕ). These maps give a directional and geographical distribution of skewness and kurtosis values calculated from a given CMB input map.

Now, the discrete functions $S(\theta_j, \phi_j)$ and $K(\theta_j, \phi_j)$ defined on the two-sphere $\mathbb{S}^2$ can be expanded into their spherical harmonics and their angular power spectra can be calculated from the corresponding coefficients. Thus, for example, for $S(\theta_j, \phi_j)$ one has

$$S(\theta_j, \phi_j) = \sum_{\ell=0}^{\infty} \sum_{m=-\ell}^{\ell} a_{\ell m}\, Y_{\ell m}(\theta, \phi), \tag{3}$$

and the corresponding angular power spectrum

$$S_\ell = \frac{1}{2\ell + 1} \sum_m |a_{\ell m}|^2. \tag{4}$$

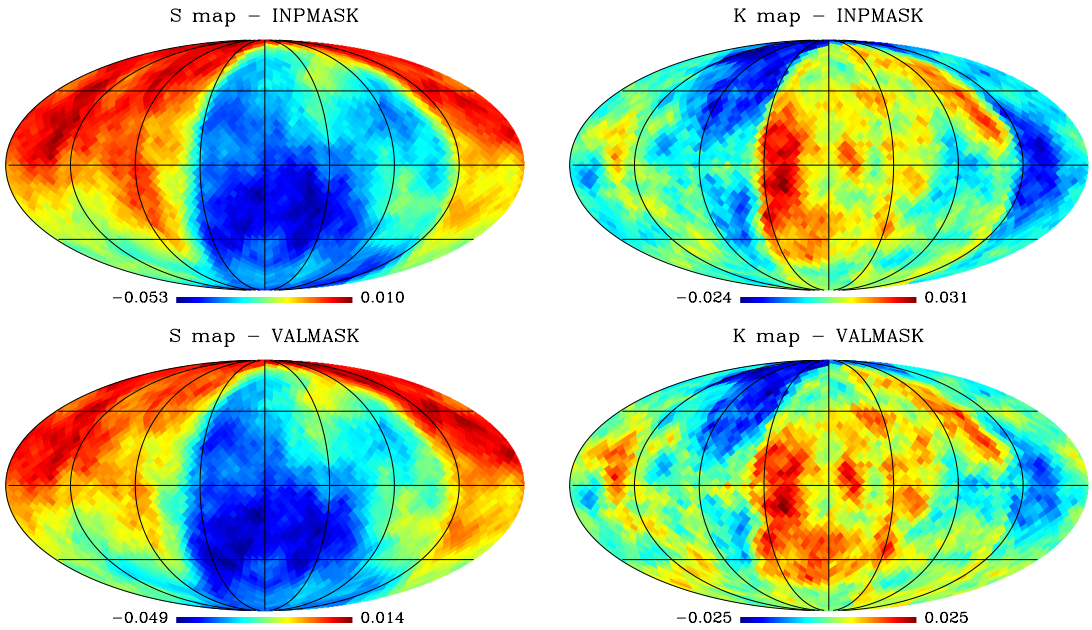

Fig. 1. S (*left*) and K (*right*) maps calculated from the SMICA map with $N_{\rm side} = 512$. The INPMASK was used for generating the maps in the first row, while in the second row the VALMASK was employed to generate the maps.

Clearly, one can similarly expand the kurtosis function $K(\theta_j, \phi_j)$ and calculate its angular power spectrum K_ℓ. Since we are interested in the large angular scale information, we restrict our analyses to the low ℓ spectra, i.e., $\ell = 1, \ldots, 10$.

In the next sections we use the power spectra S_ℓ and K_ℓ to assess possible departures from Gaussianity of the SMICA, NILC, and SEVEM foreground-cleaned *Planck* maps and to calculate the statistical significance of potential deviation from Gaussianity by comparison with the corresponding power spectra calculated from input Gaussian maps.

4. Non-Gaussianity in the *Planck* maps

The use of the non-Gaussian statistical procedure described in Sect. 3 requires not only the choice of the CMB input maps, but also specification of some important quantities that are required to carry out the computational routine. In this way, to minimize the statistical noise in the calculation of the functions $S(\theta_j, \phi_j)$ and $K(\theta_j, \phi_j)$ from *Planck* input maps, we have scanned the celestial sphere with spherical caps of aperture $\gamma = 90°$, centered at 3072 points homogeneously distributed on the two-sphere $\mathbb{S}^2$ and generated by using HEALPix package (Górski et al. 2005). This robust choice of quantities has been established in Bernui & Rebouças (2009, 2010), and thoroughly tested recently by using simulated CMB maps in Bernui & Rebouças (2012).

Figure 1 gives an illustration of S (left panels) and K (right panels) maps obtained from the foreground-cleaned SMICA *Planck* map with grid resolution $N_{\rm side} = 512$ and $\ell_{\rm max} = 500$, which we have used in the analyses of this paper. In the first row, the INPMASK was used for calculating S and K maps, while in the second row the VALMASK was employed to generate the maps[3]. These maps show distributions of hot (red) and cold (blue) spots (higher and lower values) for the skewness and kurtosis that are not evenly distributed in the celestial sphere, at first sight suggesting a large-angle multipole component of non-Gaussianity in the SMICA data, whose statistical significance we examine in detail below. A first comparison between the S maps (left panels) and between the K maps (right panels) shows several large-scale similarities between the maps in the columns in Fig. 1. To go a step further in this study, in Fig. 2 we show the result of a pixel-to-pixel comparative analysis of the pairs of S and K maps of Fig. 1. Thus, the left hand panel shows the correlation of S maps calculated from SMICA with INPMASK and VALMASK, while the right hand panel shows a similar correlation of two K maps with these masks. The panels of Fig. 2 make it apparent that the pair of S and the pair of K maps, produced from SMICA and equipped with INPMASK and VALMASK, are well-correlated, with Pearson's coefficients given by 0.961 and 0.947 for the pair of S maps and the pair K maps, respectively[4].

To obtain quantitative large angular scale information of the S and K maps obtained from foreground-cleaned *Planck* maps, we have calculated the low ℓ ($\ell = 1, \ldots, 10$) power spectra S_ℓ and K_ℓ from NILC, SMICA, and SEVEM *Planck* maps with the released INPMASK, VALMASK, and U73 masks. These power spectra can be used to access large-angle (low ℓ) deviation from Gaussianity in the *Planck* maps. To estimate the statistical significance, we collectively compare S_ℓ and K_ℓ with the multipole values of the averaged power spectra $\overline{S}^{\rm G}_\ell$ and $\overline{K}^{\rm G}_\ell$ calculated from 1000 Gaussian CMB maps, which have been obtained as stochastic realizations, with ΛCDM power spectrum, by using SYNFAST facility of the HEALPix package (Górski et al. 2005).

Figure 3 shows the power spectra S_ℓ and K_ℓ calculated from SMICA and NILC maps masked with INPMASK (first row) and VALMASK (second row)[5]. This figure also displays the points

[3] We also calculated S and K maps from the NILC and SEVEM maps with the available INPMASK, VALMASK, and U73 masks. However, to avoid repetition we only depict the maps of Fig. 1.

[4] At first glance, this could be seen as an indication that Gaussian features of the SMICA map would not change with the application of INPMASK and VALMASK. However, we show below that despite these correlations, the large-scale Gaussianity properties change appreciably with the mask used.

[5] We note that there is no available INPMASK for the SEVEM map. Thus, we have not included this map in the analysis of Fig. 3.

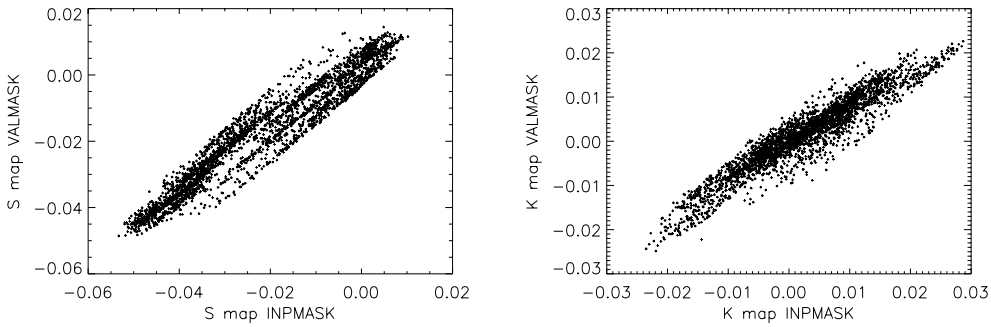

Fig. 2. Correlation between the two S maps (*left panels*) and the two K maps (*right panels*) of Fig. 1. The *left panel* presents the correlation of two S maps, one of them masked with the INPMASK, and another with VALMASK. The *right panel* shows the correlation of two K maps with the INPMASK and VALMASK. All non-Gaussian maps we employed were generated from CMB input SMICA map.

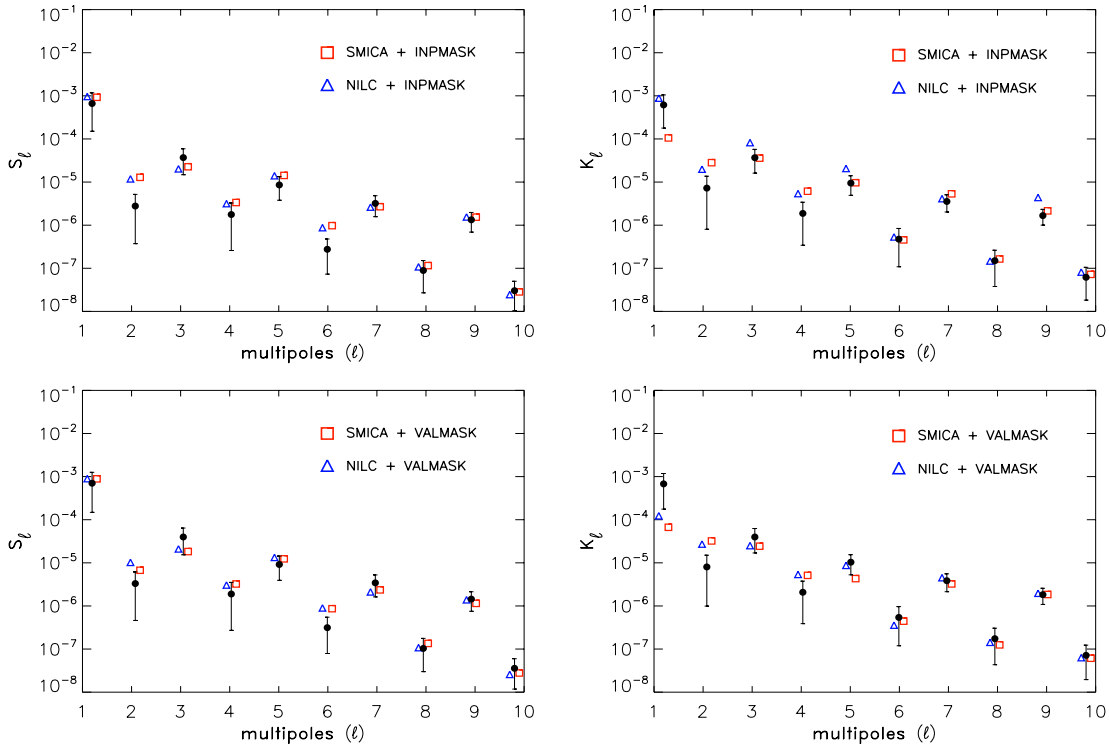

Fig. 3. Low ℓ power spectra S_ℓ (*left panels*) and K_ℓ (*right panels*) calculated from SMICA and NILC foreground-cleaned *Planck* maps equipped with INPMASK (*first row*) and VALMASK (*second row*). Tiny horizontal shifts have been used to avoid overlaps of symbols. The 1σ error bars (68.3% confidence level) are calculated from the power spectra of 1000 Gaussian maps.

of the averaged power spectra $\overline{S}^{\rm G}_\ell$ and $\overline{K}^{\rm G}_\ell$ calculated from 1000 Gaussian simulated CMB maps and the corresponding 1σ error bars. To the extent that some of power spectra values S_ℓ and K_ℓ fall off the 1σ error bars centered on $\overline{S}^{\rm G}_\ell$ and $\overline{K}^{\rm G}_\ell$ values, this figure suggests deviation from Gaussianity in both SMICA and NILC maps when masked either with INPMASK or with VALMASK. This deviation, however, seems to be substantially smaller when a more severe cut-sky is used. Indeed, in Fig. 4 it is shown that the power spectra S_ℓ and K_ℓ calculated from SMICA, NILC, and also SEVEM maps, but now with the U73 mask. This time, however, all low ℓ multipole values are within 1σ bar of the mean multipoles values obtained from simulated Gaussian maps.

Although the above comparison of the power spectra can be used as a first indication of deviation from Gaussianity of different degrees for distinct masks, to have a quantitative overall assessment of this deviation on a large angular scale, we employed the power spectra S_ℓ and K_ℓ (calculated from the foreground-cleaned *Planck* maps) to carry out a χ^2 analysis to determine the goodness of fit of these power spectra obtained from the *Planck* maps as compared to the mean power spectra calculated from simulated Gaussian maps ($\overline{S}^{\rm G}_\ell$ and $\overline{K}^{\rm G}_\ell$). Thus, for the power spectrum S_ℓ obtained from a given *Planck* map one has

$$\chi^2_{S_\ell} = \frac{1}{n-1}\sum_{\ell=1}^{n}\frac{\left(S_\ell - \overline{S}^{\rm G}_\ell\right)^2}{(\sigma^G_\ell)^2}, \tag{5}$$

where $\overline{S}^{\rm G}_\ell$ are the mean multipole values for each ℓ mode, $(\sigma^{\rm G}_\ell)^2$ is the variance calculated from 1000 Gaussian simulated maps, and n is the highest multipole one chooses to analyze the Gaussianity. We took this to be $\ell = 10$ in this paper, since we are concerned with large-angle non-Gaussianity. Obviously a similar expression and reasoning can be used for K_ℓ.

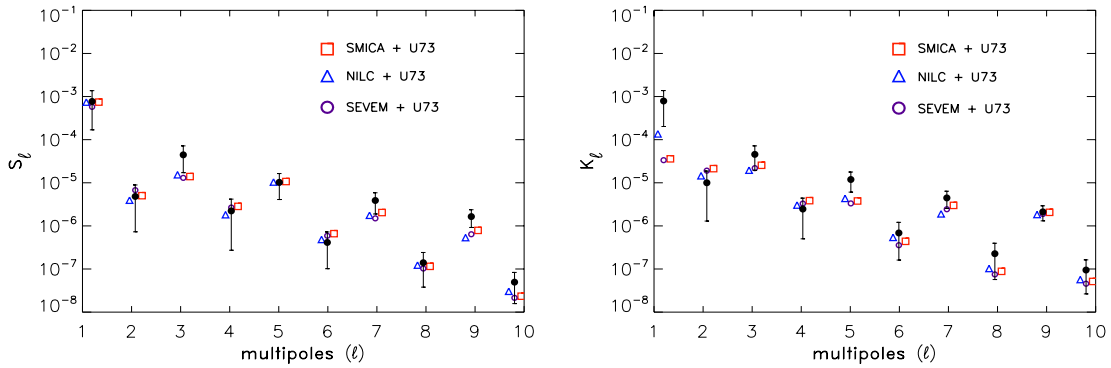

Fig. 4. Low ℓ power spectra S_ℓ (*left*) and K_ℓ (*right*) calculated from SMICA, NILC and SEVEM foreground-cleaned U73 masked maps. Tiny horizontal shifts have been used to avoid overlaps of symbols. The 1σ error bars (68.3% confidence level) are calculated from the power spectra of 1000 Gaussian maps.

Table 2. χ^2 tests for S_ℓ and K_ℓ (see text for details).

Map & Mask	$\chi^2_{S_\ell}$-probability	$\chi^2_{K_\ell}$-probability
SMICA–INPMASK	1.00×10^{-4}	1.02×10^{-2}
SMICA–VALMASK	3.74×10^{-1}	4.49×10^{-2}
NILC–INPMASK	1.80×10^{-3}	2.00×10^{-5}
NILC–VALMASK	9.95×10^{-2}	1.45×10^{-1}
SEVEM–VALMASK	8.68×10^{-1}	5.95×10^{-1}
SMICA–U73	8.43×10^{-1}	5.14×10^{-1}
NILC–U73	8.25×10^{-1}	6.27×10^{-1}
SEVEM–U73	7.29×10^{-1}	4.56×10^{-1}

Table 3. χ^2 tests for S_ℓ and K_ℓ (see text for details).

Map & Mask	$\chi^2_{S_\ell}$-probability	$\chi^2_{K_\ell}$-probability
SMICA+noise–INPMASK	3.00×10^{-4}	1.61×10^{-2}
SMICA+noise–VALMASK	4.20×10^{-1}	5.19×10^{-2}
NILC+noise–INPMASK	1.10×10^{-3}	1.00×10^{-4}
NILC+noise–VALMASK	1.15×10^{-1}	1.62×10^{-1}
SEVEM+noise–VALMASK	8.68×10^{-1}	6.16×10^{-1}
SMICA+noise–U73	8.07×10^{-1}	6.47×10^{-1}
NILC+noise–U73	8.25×10^{-1}	6.01×10^{-1}
SEVEM+noise–U73	7.55×10^{-1}	5.91×10^{-1}

The greater the χ^2 values, the lower the χ^2-probability, that is, the probability that the multipole values of a given *Planck* map S_ℓ and the mean multipole values $\overline{S}^{\rm G}_\ell$ agree. Thus, for a given *Planck* map, the $\chi^2_{S_\ell}$-probability measures its deviation from Gaussianity as detected by the indicator S. Clearly, the lower the $\chi^2_{S_\ell}$-probability, the greater the departure from Gaussianity. Again, similar procedures and statements hold for K_ℓ and the corresponding $\chi^2_{K_\ell}$-probability. In this way, for each foreground-cleaned *Planck* maps with a given mask, we can calculate statistical numbers that collectively quantify the large-angle deviation from Gaussianity as detected by our indicators S and K.

In Table 2 we collect the results of our χ^2 analyses in terms of probability for the SMICA, NILC, and SEVEM, equipped with released INPMASK, VALMASK, and the union mask U73. Concerning the SMICA and NILC, this table shows significant deviations from Gaussianity ($\gtrsim$98% confidence level) for both maps when they are masked with INPMASKs (sky-cut is 3%), which becomes smaller (with different rate) when the VALMASKs, whose sky-cuts are, respectively, 7% and 11%, are employed[6]. Table 2 also makes clear that, although with different χ^2-probabilities, the SMICA, NILC, and SEVEM masked with the union mask U73 are consistent with Gaussianity as detected by our indicator S, in agreement with the results found by the *Planck* team (Planck Collaboration XXIII 2014). Interestingly, Table 2 shows that this consistency with Gaussianity is less when the K indicator is employed in the analysis. This seems to be associated with large-angle anomalies as reported by the *Planck* team (Planck Collaboration I; XXIII 2014).

In their studies of Gaussianity, the *Planck* team has performed a large number of validation tests to examine the impact of realistic factors on their results of non-Gaussianity. Among these tests they have studied the effect of the different noise models in their estimates and produced (and released) anisotropic full-sky noise maps for SMICA, NILC, and SEVEM maps (Planck Collaboration XXIV 2014). Thus, a pertinent question that arises here is how the above analyses are impacted if one incorporates the noise estimated by the *Planck* team into their foreground-cleaned maps. To tackle this question, we calculated SMICA+noise, NILC+noise, and SEVEM+noise maps, which were then masked with INPMASK, VALMASK, and U73 masks, and used the resulting maps as input in our analyses of NG, performed through the statistical procedure of Sect. 3. In Table 3 we collected the results of our calculations. The comparison of this with Table 2 shows that the results of the analyses do not change appreciably when the noise is incorporated into the foreground-cleaned *Planck* maps.

5. Concluding remarks

The study of Gaussianity of CMB fluctuations can be used to break the degeneracy between the inflationary models and to test alternative scenarios. In most of these studies, one is particularly interested in the primordial component. However, there are several sources of non-Gaussian contaminants in the CMB data.

One does not expect that a single statistical estimator can be sensitive to all sources of non-Gaussianity that may be present in observed CMB data. On the other hand, different statistical indicators can provide valuable complementary information about different features and be useful for extracting information

[6] This comparison was not made for the SEVEM map since no INPMASK for this map has been released by the *Planck* team. We included the values of χ^2-probabilities for the SEVEM masked with VALMASK in Table 2 for completeness.

about the source of non-Gaussianity. Thus, is it important to test CMB data for Gaussianity by employing different statistical estimators.

Studies of the non-Gaussianity of the CMB temperature fluctuations data can be grouped into two classes of statistical approaches. In the first, one searches to constrain primordial non-Gaussianity parameter such as the amplitude $f_{\rm NL}$, which can be predicted from the different models of the early universe and confronted with observations. Different models give rise to different predictions (type and amplitude) for $f_{\rm NL}$. Besides allowing an optimal implementation, another advantage of this class of parametric estimators is that it is easy to compare estimates of $f_{\rm NL}$ for different models. However, the standard formulation and implementation of the estimator $f_{\rm NL}$ has been designed under the assumption of statistical isotropy of the CMB sky. The second class contains statistical tools designed to search for non-Gaussianity in the CMB maps regardless of its origin. The surrogate map technique used by *Planck* team and our S and K indicators are examples of the statistical procedures in this class. The indicators of this class have the advantage of being model-independent, since no particular model of the early universe is assumed in their formulation and practical implementation. However, with these model-independent tools, one cannot immediately insure whether a detection of non-Gaussianity in CMB data is of primordial origin. This makes the problem of finding the connection between statistical tools in these two classes a difficult theoretical task.

The *Planck* team has examined Gaussianity in CMB data by using various different statistical tools and approaches. Among others, they have employed one of the simplest tests for Gaussianity of CMB data by calculating a sample of values of skewness S and kurtosis K from the whole set of accurate temperature fluctuations values of their foreground-cleaned U73-masked maps, and made a comparison with the averaged values for the statistical moments calculated from simulated maps (Planck Collaboration XXIII 2014).

In this work we have gone a step further, and instead of using two dimensionless overall numbers, we employed a procedure for defining, from a CMB map, two discrete functions $S(\theta_j, \phi_j)$ and $K(\theta_j, \phi_j)$, which measure directional deviation from Gaussianity, for $j = 1, \ldots, 3072$ homogeneously distributed directions, (θ_j, ϕ_j), on the two-sphere $\mathbb{S}^2$. The Mollweide projections of these two functions are skewness and kurtosis maps, whose low ℓ power spectra has been used to investigate large-angle deviation from Gaussianity in *Planck* data. These estimators capture directional information of non-Gaussianity and are useful, for instance, in the presence of anisotropic signals such as residual foregrounds.

This statistical procedure has been recently proposed (Bernui & Rebouças 2009) and used in connection with foreground-reduced WMAP maps (Bernui & Rebouças 2010; Zhao 2013). A significant deviation from Gaussianity has been found in the WMAP foreground-reduced maps, which varies with the cleaning processes (Hinshaw et al. 2009; Kim et al. 2008; Delabrouille et al. 2009).

This paper addressed several interrelated issues regarding these skewness-kurtosis spherical caps procedure in connection with large-angle non-Gaussianity in the foreground-cleaned *Planck* maps. First, we used these statistical estimators to analyze the Gaussianity of the nearly full-sky foreground-cleaned *Planck* maps, therefore extending the results of Bernui & Rebouças (2010). Second, we made statistical analyses of the effects of different component separation cleaning methods in the Gaussianity, and quantified the level of non-Gaussianity for each foreground-cleaned *Planck* maps equipped with each the released INPMASK, VALMASK, and U73 masks (see Table 1). Third, we used the pixel's noise maps released by the *Planck* team to examine the robustness of the Gaussianity analyses with respect to this noise. The main results of our analyses are summarized in Tables 2 and 3, together with Figs. 1 to 4.

Figure 1 illustrates skewness (left) and kurtosis (right) maps obtained from the SMICA *Planck* maps with INPMASK (first row) and VALMASK (second row). The panels of Fig. 2 illustrate how well the pair of S maps are correlated, as are the pair of K maps of Fig. 1.

The power spectra S_ℓ and K_ℓ of the maps in Fig. 3 indicate deviation from Gaussianity in both SMICA and NILC maps when masked with either INPMASK or VALMASK. This deviation, however, is substantially reduced when a more severe cut-sky is employed as shown in Fig. 4, wherein all low ℓ multipole values are within 1σ bar of the mean multipoles values obtained from simulated Gaussian maps.

The comparison of Fig. 3 with Fig. 4 furnishes rough indications of deviation from Gaussianity on a large angular scale and the role played by the different *Planck* masks. However, we made quantitative overall assessments of this large-angle deviation through χ^2 analyses and determined the goodness of fit of the power spectra obtained from the *Planck* maps as compared to the mean power spectra calculated from simulated Gaussian maps.

In Table 2 we collected the results of our χ^2 analyses in terms of probability. Concerning the SMICA and NILC, this table shows significant deviations from Gaussianity for both maps when they are masked with their INPMASKs (sky-cut is only 3%), which becomes smaller when the VALMASKs, whose sky-cuts are 7% and 11%, are employed. We emphasize that Table 2 also shows that – although to different degrees – the SMICA, NILC, and SEVEM masked with the union mask U73 are consistent with Gaussianity as detected by our indicator S, in agreement with the results obtained by the *Planck* team, but through different statistical procedures (Planck Collaboration XXIII 2014). However, a slightly smaller consistency with Gaussianity has been found when the K indicator is employed, which seems to be associated with the large-angle anomalies reported by the *Planck* team (Planck Collaboration XXIII 2014).

We also addressed the question of how the results of Gaussianity analyses are modified when the noise is added to the foreground-cleaned *Planck* maps, a point that has not been considered in Planck Collaboration XXIII (2014). Tables 2 and 3 show that the results of the analyses do not change appreciably when the noise is incorporated into the *Planck* maps.

Finally, we note that by using simulated maps in Bernui & Rebouças (2012), we showed that the indicators S and K do not have enough sensitivity to detect tiny primordial non-Gaussianity. This amounts to saying that any significant detection of non-Gaussianity through the S and K should contain a non-primordial contribution. This makes clear that these indicators can be used to capture non-Gaussianity components of non-primordial origin that may be present in foreground-cleaned maps. Furthermore, S and K indicators have the advantage of providing angular variation (directional information) of non-Gaussianity of the maps and also deal with the large-angular scale features of non-Gaussianity.

Acknowledgements. M.J. Rebouças acknowledges the support of FAPERJ under a CNE E-26/102.328/2013 grant. This work was also supported by Conselho Nacional de Desenvolvimento Científico e Tecnológico (CNPq) – Brasil, under Grant No. 475262/2010-7. M.J.R. and A.B. thank the CNPq for the grants under

which this work was carried out. We are also grateful to A.F.F. Teixeira for reading the manuscript and indicating the omissions and misprints. We acknowledge the use of the *Planck* data. Some of the results in this paper were derived using the HEALPix package (Górski et al. 2005).

References

Ade, P. A. R., Aikin, R. W., Barkats, D., et al. 2014, Phys. Rev. Lett., 112, 1101
Albrecht, A., & Steinhardt, P. J. 1982, Phys. Rev. Lett., 48, 1220
Bartolo, N., Komatsu, E., Matarrese, S., & Riotto, A. 2004, Phys. Rept., 402, 103
Bassett, B. A., Tsujikawa, S., & Wands, D. 2006, Rev. Mod. Phys., 78, 537
Bennett, C. L., Hill, R. S., Hinshaw, G., et al. 2003, ApJS, 148, 97
Bernui, A., & Rebouças, M. J. 2009, Phys. Rev. D, 79, 3528
Bernui, A., & Rebouças, M. J. 2010, Phys. Rev. D, 81, 3533
Bernui, A., & Rebouças, M. J. 2012, Phys. Rev. D, 85, 3522
Bernui, A., Mota, B., Rebouças, M. J., & Tavakol, R. 2007, A&A, 464, 479
Buchbinder, E. I., Khoury, J., & Ovrut, B. A. 2008, Phys. Rev. Lett., 100, 1302
Cai, Y.-F., Xue, W., Brandenberger, R., & Zhang, X. 2009a, JCAP, 05, 011
Cai, Y.-F., Xue, W., Brandenberger, R., & Zhang, X. 2009b, JCAP, 06, 037
Cardoso, J.-F., Martin, M., Delabrouille, J., Betoule, M., & Patanchon, G. 2008, IEEE J. Select. Topics Signal Process., 2, 735
Creminelli, P., & Zaldarriaga, M. 2004, JCAP, 10, 006
Curto, A., Macís-Pérez, J. F., Martínez-González, E., et al. 2008, A&A, 486, 383
Delabrouille, J., Cardoso, J.-F., Le Jeune, M., et al. 2009, A&A, 493, 835
Donzelli, S., Hansen, F. K., Liguori, M., & Maino, D. 2009, ApJ, 706, 1226
Fernández-Cobos, R., Vielva, P., Barreiro, R. B., & Martínez-González, E. 2012, MNRAS, 420, 2162
Flauger, R., Hill, J. C., & Spergel, D. N. 2014, JCAP, 08, 039
Goldberg, D. M., & Spergel, D. N. 1999, Phys. Rev. D, 59, 3002
Górski, K. M., Hivon, E., Banday, A. J., et al. 2005, ApJ, 622, 759
Gott, J. R. I., Park, C., Juszkiewicz, R., et al. 1990, ApJ, 352, 1
Guth, A. H. 1981, Phys. Rev. D, 23, 347
Eriksen, H. K., Novikov, D. I., Lilje, P. B., Banday, A. J., & Górski, K. M. 2004, ApJ, 612, 64
Hinshaw, G., Weiland, J. L., Hill, R. S., et al. 2009, ApJS, 180, 225
Kazanas, D. 1980, ApJ, 241, L59
Kim, J., Naselsky, P., & Christensen, P. R. 2008, Phys. Rev. D, 77, 3002
Komatsu, E. 2010, Class. Quant. Grav., 27, 4010
Komatsu, E., Kogut, A., Nolta M. R., et al. 2003, ApJS, 148, 119
Komatsu, E., Dunkley, J., Nolta, M. R., et al. 2009, ApJS, 180, 330
Komatsu, E., Afshordi, N., Bartolo, N., et al. 2009, Cosmology and Fundamental Physics Science Frontier Panel, submitted [arXiv:0902.4759v4]
Koyama, K., Mizuno, S., Vernizzi, F., & Wands, D. 2007, JCAP, 11, 024
Leach, S. M., Cardoso, J.-F., Baccigalupi, C., et al. 2008, A&A, 491, 597
Lehners, J.-L., & Steinhardt, P. J. 2008, Phys. Rev. D, 77, 3533
Lewis, A., & Challinor, A. 2006, Phys. Rep., 429, 1
Linde, A. 2008, Lect. Notes Phys., 738, 1
Linde, A. D. 1982, Phys. Lett. B, 108, 389
Martínez-González, E., Gallegos, J. E., Argüeso, F., Cayón, L., & Sanz, J. L. 2002, MNRAS, 336, 22
Minkowski, H. 1903, Math. Ann., 57, 447
Modest, H. I., Räth, C., Banday, A. J., et al. 2013, MNRAS, 428, 551
Novaes, C. P., & Wuensche, C. A. 2012, A&A, 545, A34
Novaes, C. P., Bernui, A., Ferreira, I. S., & Wuensche, C. A. 2014, JCAP, 01, 018
Planck Collaboration I. 2014, A&A, 571, A1
Planck Collaboration XII. 2014, A&A, 571, A12
Planck Collaboration XXIII. 2014, A&A, 571, A23
Planck Collaboration XXIV. 2014, A&A, 571, A24
Planck Collaboration XXX. 2015, A&A, accepted [arXiv:1409.5738]
Rees, M. J., & Sciama, D. W. 1968, Nature, 217, 51
Rassat, A. , Starck, J.-L., Paykari, P., Sureau, F., & Bobin, J. 2014, JCAP, 08, 006
Räth C., Morfill G. E., Rossmanith G., Banday A. J., & Górski, K. M. 2009, Phys. Rev. Lett., 102, 1301
Räth, C., Banday, A. J., Rossmanith, G., et al. 2011, MNRAS, 415, 2205
Sato, K. 1981, MNRAS, 195, 467
Starobinsky, A. A. 1979a, JETP Lett., 30, 682
Starobinsky, A. A. 1979b, Pisma Zh. Eksp. Teor. Fiz., 30, 719
Starobinsky, A. A. 1982, Phys. Lett. B, 117, 175
Su, M., Yadav, A. P. S., Shimon, M., & Keating, B. G. 2011, Phys. Rev. D, 83, 3007
De Troia, G., Ade, P. A. R., Bock, J. J., et al. 2007, ApJ, 670, L73
Zel'dovich, Y. B., & Sunyaev, R. A. 1969, Astrophys. Space Sci., 4, 301
Zhao, W. 2013, MNRAS, 433, 3498